Thermal Conductivity of Nanoporous Silicon: Molecular Dynamics Simulations and Machine Learning Prediction

V.V. Kuryliuk (0000-0003-0898-8888), O.Ya. Olikh (0000-0003-0633-5429)

Taras Shevchenko National University of Kyiv, 60 Volodymyrska Street, Kyiv, Ukraine, 01033

kuryliuk@knu.ua, olegolikh@knu.ua

Abstract

The thermal conductivity of nanoporous silicon (p-Si) was investigated using equilibrium molecular dynamics simulations and machine learning techniques. Several interatomic potentials were evaluated, with the Tersoff potential selected for its stability and accuracy. Thermal conductivity values were computed over a wide range of temperatures and porosities. A algorithm was used to derive an analytical expression describing its dependence on temperature and porosity. Additionally, Random Forest and Gradient Boosting models were trained to reconstruct heat current autocorrelation functions and predict thermal conductivity, outperforming Support Vector Regression. The combined approach enables accurate, data-efficient prediction of thermal transport in porous nanostructures, supporting the design of materials for thermal management and energy conversion applications.

Keywords: *nanoporous silicon, thermal conductivity, molecular dynamics, symbolic regression, machine learning*

Introduction

In recent years, nanostructured materials have attracted significant interest for their potential in thermal insulation and heat dissipation applications [1, 2]. For instance, as 3D integration advances in micro- and nanoelectronics, there is a growing need for low thermal conductivity materials that remain compatible with CMOS processes. Furthermore, for energetically autonomous systems, the development of effective nanomaterials exhibiting high thermoelectric conversion efficiency is also crucial [3]. The thermal behavior of nanomaterials is significantly influenced by their structural dimensions and the manner in which phonons propagate through their frameworks [4]. In such materials, thermal phonons are frequently scattered at surfaces and interfaces, thereby significantly lowering overall thermal conductivity [5]. It is noteworthy that nanoporous structures have attracted significant interest due to their large specific surface area and shortened phonon mean free path, which further suppresses heat transport [6, 7].

Nanoporous silicon (*p*-Si), produced by electrochemical anodization of crystalline silicon, has attracted significant attention because its optical, electrical, and thermal properties can be readily tuned by adjusting the porosity. This controllability enables a wide range of potential applications

for p-Si in areas such as highly sensitive sensors [8], lithium-ion batteries [9], optoelectronics, micro- and nanoelectronics [10], as well as MEMS technologies [11]. It has been demonstrated that nanostructured silicon with tailored porosity exhibits thermal conductivity that is two to three orders of magnitude lower than that of bulk crystalline silicon ($\sim$140 W$\cdot$m$^{-1}\cdot$K^{-1}) [12]. This renders it an appealing candidate for utilization in thermal sensors [13], thermal insulation and thermoelectric generators in silicon-based microsystems [14]. In order to gain deeper insight into the mechanisms of phonon transport in p-Si, it is crucial to undertake comprehensive thermal characterization. Furthermore, it is imperative to possess precise knowledge of the thermal behavior of this material to ensure its effective integration into practical devices.

Molecular dynamics (MD) simulations have become an indispensable tool for investigating thermal transport phenomena in nanostructured materials, providing valuable atomistic insights that are often inaccessible through experiments alone. In particular, MD methods have been extensively utilized to predict the thermal conductivity of porous silicon and analogous systems, elucidating the profound impact of nanoscale characteristics, such as pore size, shape, and distribution, on phonon scattering and heat conduction [15-18]. The integration of machine learning (ML) approaches with atomistic modelling has emerged as a promising strategy to efficiently predict and optimize the properties of complex materials by uncovering hidden structure-property relationships. Two primary approaches integrate ML with MD. The first one employs machine learning interatomic potentials in simulations, enabling the study of large-scale emergent phenomena in specific materials with accuracy close to that of ab initio MD [19, 20]. The second approach uses MD simulation results from a limited number of cases as input data to build and train ML models; these models are then applied to a much wider range of predictions [21, 22]. Both methods have been successfully used to assess the thermal properties of various materials [23-27], including porous structures [28]. As previous studies have shown that such integrated frameworks can significantly accelerate the design of advanced nanostructured materials for thermal management and energy conversion applications. Unfortunately, to the best of our knowledge, no similar studies have been conducted on porous silicon.

In this study, molecular dynamics and machine learning methods were employed to calculate the thermal conductivity of nanoporous silicon. A series of interatomic interaction potentials were tested to predict heat transport in silicon. The equilibrium molecular dynamics approach was used to determine the dependence of the thermal conductivity on temperature and porosity. The resulting dataset was then processed and generalized using machine learning models, allowing the thermal conductivity of p-Si to be estimated over a wide range of temperatures and porosities.

Methods

The thermal conductivity of the *p*-Si was calculated via equilibrium molecular dynamics (EMD). All MD simulations were performed using the LAMMPS package [29]. The EMD simulation setup considered in this paper is schematically illustrated in Fig. 1. The simulation box is a cube consisting of $L^3 = 10a \times 10a \times 10a$ unit cells, where *a* is the unit-cell lattice vector in the Si. The porosity of the structure was varied by changing the pore radius *R* and was calculated as $\eta = \dfrac{4\pi R^3}{3L^3}$.

The pore was introduced as a spherical cavity by removing atoms from the silicon lattice and was placed at the center of the simulation box to ensure symmetry and minimize boundary effects. While real materials often exhibit randomly distributed pores of irregular shape, modern fabrication techniques also enable periodic porous structures [30, 31]. For each temperature and porosity, an initial simulation was performed in the isobaric–isothermal (NPT) ensemble to generate thermally equilibrated configurations. The system was then further equilibrated in an isochoric–isothermal (NVT) ensemble. In both the NPT and NVT simulations, the temperature was controlled using a Nosé–Hoover thermostat. The simulation time for each ensemble was 0.5 ns, and the integration of Newton's equations of motion was carried out using the Verlet algorithm with a time step of 1 fs. After reaching equilibrium, the system was switched to a constant-volume and constant-energy (NVE) ensemble to determine the thermal conductivity *k* using the Green–Kubo method. In this method *k* was estimated by integrating the heat current autocorrelation function (HCACF) as follows:
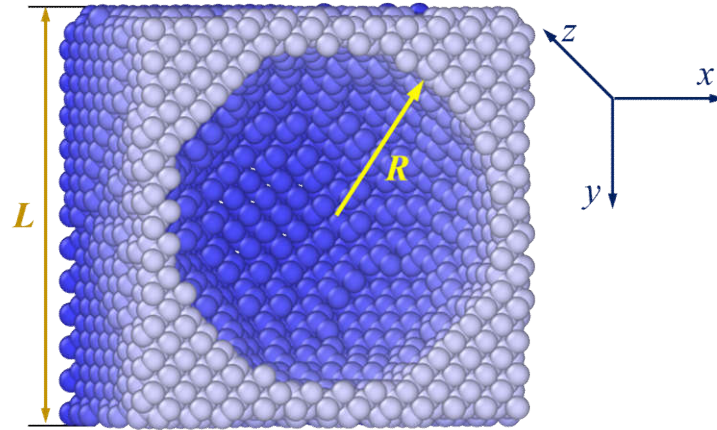

Figure 1. Schematic illustration of the EMD simulation setup: *L* – size of the Si supercell (cube), *R* – pore radius.

$$k = \frac{1}{3Vk_BT^2}\int_0^{t_c}\langle \mathbf{J}(t)\mathbf{J}(0)\rangle dt, \tag{1}$$

where *V* is the volume of the system, *t* is the time, the brackets $\langle\ \rangle$ is the ensemble-averaged HCACF and $\mathbf{J}$ is the heat current vector that is defined as

$$\mathbf{J}(t) = \frac{1}{V}\left[\sum_{j=1}^{N}\mathbf{\upsilon}_{j}E_{j} - \sum_{\alpha=1}^{2}h_{\alpha}\sum_{j=1}^{N_{\alpha}}\mathbf{\upsilon}_{\alpha j}\right] + \frac{1}{V}\left[\frac{1}{2}\sum_{j=1}^{N}\sum_{\substack{j=1,\\j\neq i}}^{N}\mathbf{r}_{ij}\left(\mathbf{\upsilon}_{ij}\cdot\mathbf{F}_{ij}\right)\right], \tag{2}$$

Here, $\mathbf{\upsilon}_j$ and E_j are the velocity and energy of the j-th particle; $\mathbf{r}_{ij}$ and $\mathbf{F}_{ij}$ denote the distance and the interaction force between the i-th and j-th particles; N is the total number of particles in the system; and h_α is the average partial enthalpy of component α. Obviously, that t_c value (the upper limit of the integral or the MD simulation time) must be sufficiently large for the system to reach equilibrium. In essence, the thermal conductivity k was determined as the saturation value of the $k(t_c)$ curve. To reduce statistical errors, our MD simulations were run for more than 10 ns on average, and five independent simulations were performed for each specific condition. For a structure with a given porosity, calculating the thermal conductivity on a cluster of 128 AMD EPYC cores at the same temperature typically took 10–12 hours.

The primary goal of applying Machine Learning (ML) methods was to enable the rapid estimation of the thermal conductivity of porous silicon across arbitrary values of porosity p ($0 \leq p < 1$) and temperature T. A key consideration when selecting ML approaches is the limited availability of thermal conductivity data – only a few dozen values can realistically be obtained from MD simulations within a feasible timeframe for model development. As a result, conventional ML methods that require training dataset containing tens or hundreds of thousands of samples are not suitable in this context.

As a result, two distinct approaches were used. The first approach employed Symbolic Regression (SR), an algorithm that derives a mathematical expression to describe a given dataset. Unlike conventional regression methods, which require predefined input variables and adjust numerical coefficients to achieve the best fit, SR simultaneously identifies both the structure of the equation and its parameters [32]. It uses evolutionary algorithms to uncover functional relationships and numerical coefficients between input and output variables. A key advantage of SR is its ability to produce interpretable results in the form of analytical expressions. Moreover, this method does not require large amounts of training data to achieve high predictive accuracy [32, 33].

SR was implemented in Python using the open-source PySR package [34]. Data preprocessing was limited to normalizing temperature values to 300 K. During training, the loss function was defined as the mean weighted squared error (MWSE) and was minimized:

$$\text{MWSE} = \frac{1}{N}\sum_{i=1}^{N}\omega_i\left(\hat{y}_i - y_i\right)^2. \tag{3}$$

Here, N represents the number of values in the training set, y_i denotes the true thermal conductivity (result of MD simulation), while $\hat{y}_i$ indicates the predicted value; ω_i is the weighting coefficient, in this study, statistical (reciprocal) weighting was applied, meaning $\omega_i = 1/y_i$. The use of weighting coefficients is motivated by the fact that the range of target values for thermal conductivity (TC)

In the second approach, classical algorithms – specifically Random Forest (RF), Gradient Boosting (GB), and Support Vector Regression (SVR) – were used to build models predicting the $k(t_c)$ curve. This strategy significantly increased the size of the training dataset. The input descriptor set included porosity, temperature, and simulation time. To standardize the features and target values, they were normalized to have zero mean and unit standard deviation. The models were implemented using Python's Scikit-learn toolkit. Model parameters were optimized using the Optuna framework, which employed the TPE sampler and Hyperband pruner for efficient hyperparameter selection. A 5-fold cross-validation scheme was applied during model tuning. To determine thermal conductivity, the predicted $k(t_c)$ curves were processed in the same way as those obtained from MD simulations.

The evaluation metrics used to assess forecast quality were the mean squared error (MSE), mean absolute percentage error (MAPE), and coefficient of determination (R^2), as defined in Eqs. (4)-(6).

$$\text{MSE} = \frac{1}{N}\sum_{i=1}^{N}(\hat{y}_i - y_i)^2, \tag{4}$$

$$\text{MAPE} = \frac{1}{N}\sum_{i=1}^{N}\frac{|\hat{y}_i - y_i|}{y_i}\times 100\%, \tag{5}$$

$$R^2 = 1 - \frac{\sum_{i=1}^{N}(\hat{y}_i - y_i)^2}{(\hat{y}_i - \overline{y})^2}, \tag{6}$$

where $\overline{y}$ is the mean of the true values. MSE was used for model tuning, while all three metrics were applied to evaluate the prediction quality of the trained models.

Results and discussion

1. *Evaluation and Selection of Interatomic Potentials.* The accuracy of MD simulations strongly depends on the choice of interatomic potential. Therefore, the initial stage of this study focused on evaluating several well-known potentials based on three key criteria: (i) computational performance, which is particularly relevant for high-throughput simulations and machine learning dataset generation; (ii) agreement between simulated and experimental temperature-dependent thermal conductivity of singlecrystalline silicon; and (iii) potential stability for highly porous structures over a wide temperature range. Clearly, the latter criterion plays the most significant role in selecting an interatomic potential for calculating the thermal properties of a porous material. The tested potentials included MEAM [35], Tersoff [36], EDIP [37], Stillinger-Weber (SW) [38],

modified Stillinger-Weber (SW-mod) [39], and a machine learning-based potential SNAP [40]. The results are summarized in Figures 2 and 3.

As shown in Figure 2, the EDIP potential demonstrated the highest computational performance, reaching nearly 5000 MD steps per second on a 128-core node. Tersoff, SW, and SW-mod potentials achieved approximately 3000 steps per second, while MEAM exhibited ten times lower performance than EDIP. The SNAP potential was the slowest, with only ~30 steps per second under identical simulation and hardware conditions.
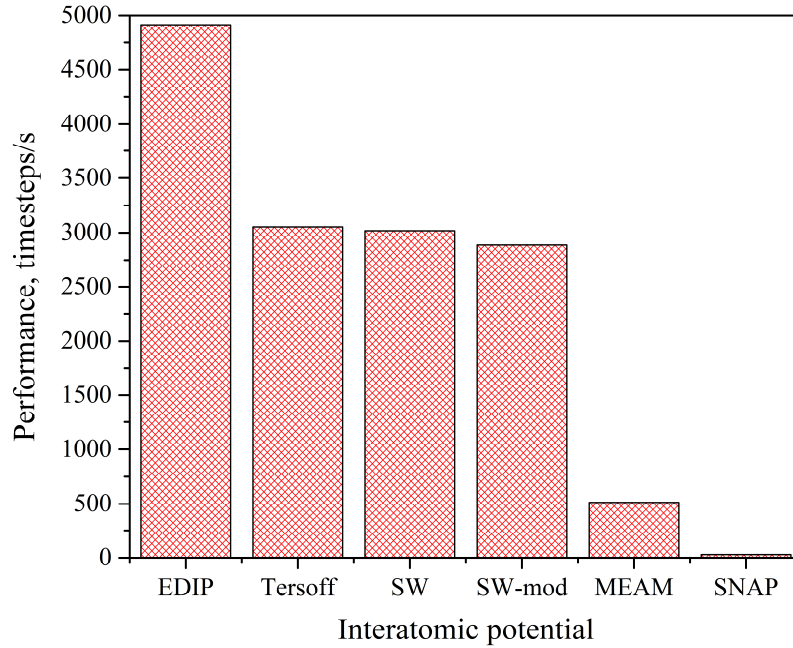

Figure 2. Comparison of the computational performance of various interatomic potentials for calculating the thermal conductivity of singlecrystalline silicon. Structure size: $10a \times 10a \times 10a$; number of cores per node: 128.
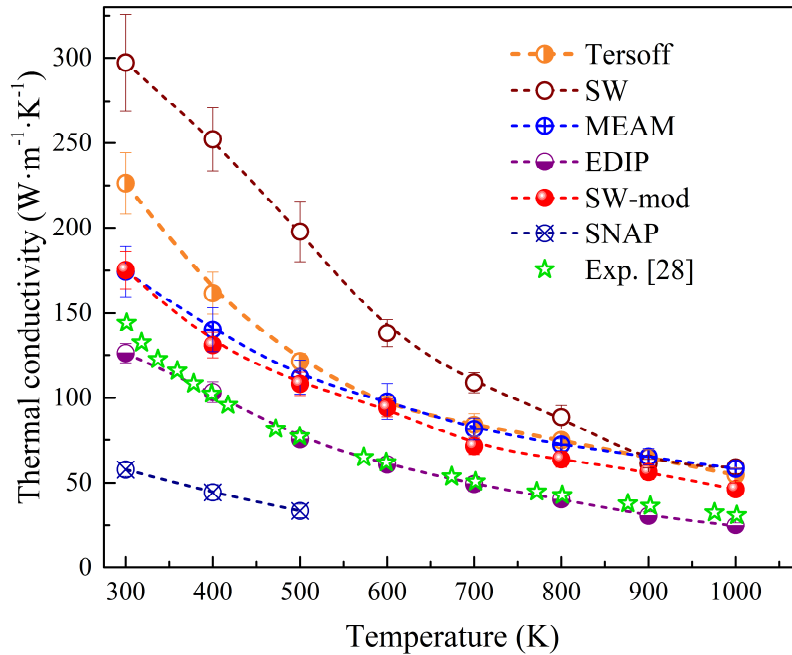

Figure 3. Calculated temperature dependence of thermal conductivity of singlecrystalline silicon using different interatomic potentials, compared with experimental data adapted from [41].

Thermal conductivity values calculated using MEAM, Tersoff, SW, and SW-mod consistently exceeded the experimental results reported in Ref. [41] across the entire temperature range, with deviations ranging from 48% to 106%. In contrast, the SNAP potential significantly underestimated the thermal conductivity, indicating inadequate parameterization for heat transport simulations. The smallest deviation between the calculated and experimental $k(T)$ dependencies was obtained using the EDIP potential. However, this should not be regarded as an inherent advantage of EDIP, since thermal conductivity calculated via MD simulations is typically higher than experimental values due to the use of idealized model structures – defect-free and mono-isotopic.

Moreover, further testing of the potentials revealed that, for highly porous structures at elevated temperatures, the porous architecture became unstable with certain potentials, leading to pore collapse and the formation of nearly amorphous configurations – see Figure 4. As shown in Table 1, similar instabilities were observed for the SW, SW-mod and EDIP potentials.
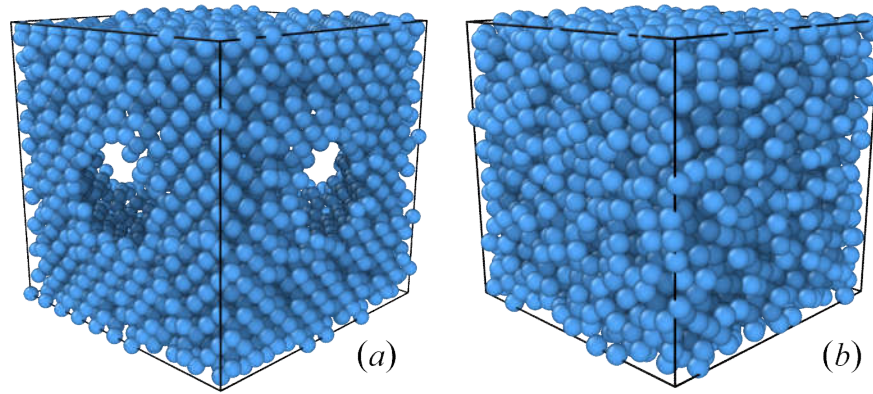

(a) (b)

Figure 4. Atomic configurations of porous silicon with 50% porosity, obtained after structure equilibration at 800 K using Tersoff potentials (a) and EDIP (b).

Table 1. Stability of interatomic potentials in MD simulations of thermal conductivity for p-Si

Potential	Stability
MEAM	+
Tersoff	+
EDIP	-
Stillinger-Weber	-
modified Stillinger-Weber	-
SNAP	+

As a result, the Tersoff potential was chosen for the remainder of the study. An additional argument in favor of Tersoff is that fitting the calculated $k(T)$ dependence for monocrystalline Si with the function $k=AT^{-b}$ yielded a value of $b=1.15\pm0.03$, which is close to the theoretical

expectation b=1.0 for semiconductors and dielectrics (for EDIP 1.36±0.09, SW 1.5±0.1, SW-mod 1.08±0.05, MEAM 0.92±0.02).

2. *Generation of Molecular Dynamics Data for Machine Learning.* The next stage of the study involved generating a dataset of MD simulation results for training machine learning models aimed at predicting the thermal properties of porous silicon structures. Two competing requirements had to be balanced. On the one hand, the simulated data needed to span a wide range of porosity and temperature values and capture all key dependencies of thermal conductivity on these parameters. On the other hand, limitations in computational resources had to be considered. Therefore, MD simulations were performed to obtain temperature-dependent thermal conductivity values at several porosity levels using 100 K intervals, as well as the dependence of thermal conductivity on pore volume fraction at room temperature. Figures 5a present selected results for the temperature and porosity dependence of thermal conductivity, calculated using the Tersoff potential.
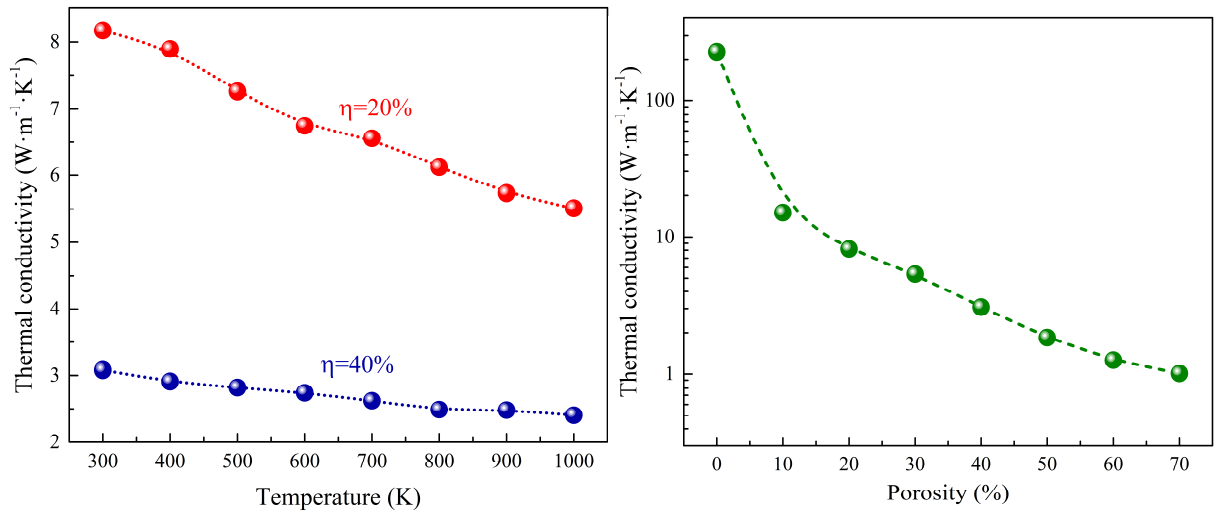

Figure 5. Dependence of thermal conductivity on temperature for *p*-Si with 20% and 40% porosity (a) and on porosity for *p*-Si at *T*=300 K porosity (b). Calculations were performed using the Tersoff interatomic potential.

It should be noted that the observed trends are consistent with literature data: thermal conductivity decreases with increasing temperature, and the form of the $k(T)$ dependence evolves as the system becomes increasingly disordered. Specifically, the exponent b in the empirical relation $k=AT^{-b}$ decreases with porosity (1.15±0.03, 0.34±0.02, and 0.21±0.01 for porosity values of 0, 0.2, and 0.4, respectively), indicating enhanced phonon scattering due to partial amorphization. A monotonic decrease in thermal conductivity with increasing porosity is also observed (Fig. 5b), attributed to increased phonon-boundary scattering at pore surfaces. Thus, this dependency aligns with general expectations, further supporting the validity of the performed calculations.

The resulting data served as a foundation for the development and training of ML models for predicting the heat transport behavior of porous silicon.

3. *Machine Learning-Based Prediction of Thermal Transport Properties in Porous Silicon.*

Using the results of MD simulations with the Tersoff potential (Figs. 3–5) and the Symbolic Regression algorithm, we derived an analytical expression describing the dependence of porous silicon's thermal conductivity on temperature and porosity. By adjusting parameters such as the population size, the maximum expression complexity, and the multiplicative coefficient penalizing complexity, we obtained a formula with a MAPE of no more than 2.89% and a median APE of 1.96% on the training set (see Fig. 6a). The resulting analytical expression is:

$$k = \left(-7.024 + \frac{7.481}{p^{0.55} + (T_n - 0.105)/(\sin[T_n/(4.486 \cdot p - 0.251)] + 27.09)} \right) \exp(-p), \quad (7)$$

where $T_n = T/300$. Figure 6b presents the obtained $k(T, p)$ dependence within the temperature range of 100–300 K and the porosity range of 0–80%. The corresponding MD simulation results are also shown in the figure.
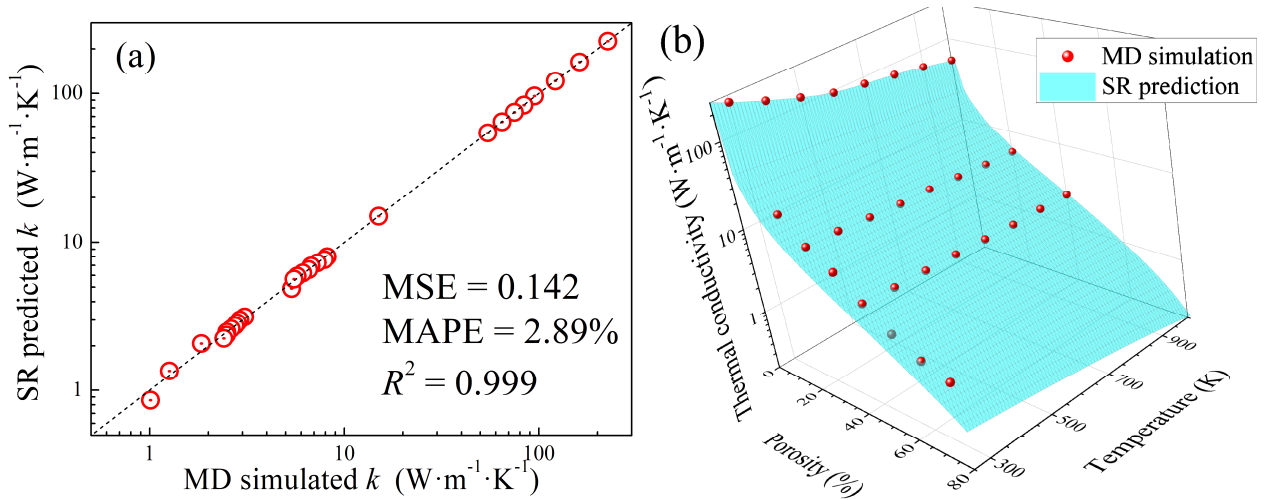

Figure 6. (a) Comparison of SR predicted k and MD calculated k (true value) for *p*-Si. The black lines are the identified lines serving as the references. (b) Dependence of the thermal conductivity of porous silicon on temperature and porosity. The spheres represent the results of MD simulations, while the surface corresponds to Eq. (7).

The initial data for each point in Figs. 3–5 consisted of MD simulation results for k at 10,000 values of t_c. This dataset was split into training (80%) and test (20%) subsets and used for developing the ML models. The training results are shown in Fig. 7. It is evident that the

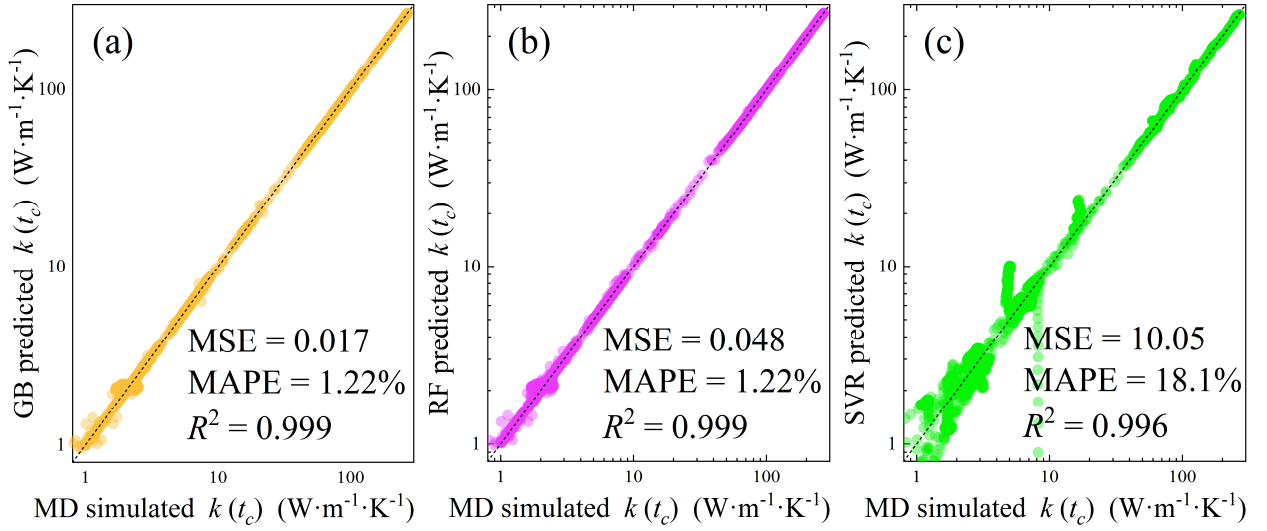performance metrics of SVR are lower than those of RF and GB, which demonstrate similar levels of accuracy.

Figure 7. Comparison of k values at different t_c, calculated by MD simulations and predicted by Gradient Boosting (a), Random Forest (b), and Support Vector Regression (c) for the training dataset. The black lines indicate reference lines.

Figure 8a presents an example of the $k(t_c)$ dependencies obtained from both MD simulations and trained ML models for the same values of T and p used during training. It is clear that RF and GB accurately reproduce the $k(t_c)$ behavior, yielding thermal conductivity values with errors below 1% when derived from the ML-generated curves. The performance of SVR is notably poorer. Overall, for thermal conductivity predictions at temperature and porosity values where MD calculations are available, the MAPEs are 1.05%, 0.98%, and 26.8%, while the R^2 values are 0.999, 0.999, and 0.977 for GB, RF, and SVR, respectively.

However, the primary objective of developing these models is to estimate thermal conductivity for values of T and p beyond the scope of MD simulations. Figure 8b presents representative $k(t_c)$ curves generated by the models, alongside MD results for similar temperature and porosity values. The curves produced by both tree-based algorithms: i) closely match each other, ii) follow trends consistent with MD results, and iii) yield thermal conductivity values that align with general expectations – that is, increasing temperature and porosity lead to lower k values. In contrast, the SVR-generated curve fails to reproduce these desirable features.

ML models were employed to estimate thermal conductivity values for various (T, p) pairs not covered by MD simulations (see Fig. 9). For comparison, values obtained using Eq. (7) are also shown in the figure as surface plots. Since no MD results are available for these temperature and porosity combinations, the evaluation metrics were computed relative to the predictions of the SR model. The small training set errors indicate that SR provides a sufficiently reliable approximation

of the physical dependence. Therefore, comparing the predictions of other ML models with Eq. (7) offers a meaningful assessment of their ability to generalize training data. This does not fully replace testing on MD or other data, but it clearly demonstrates the behavior and physical plausibility of model predictions across a wide parameter range where direct calculations are not available.
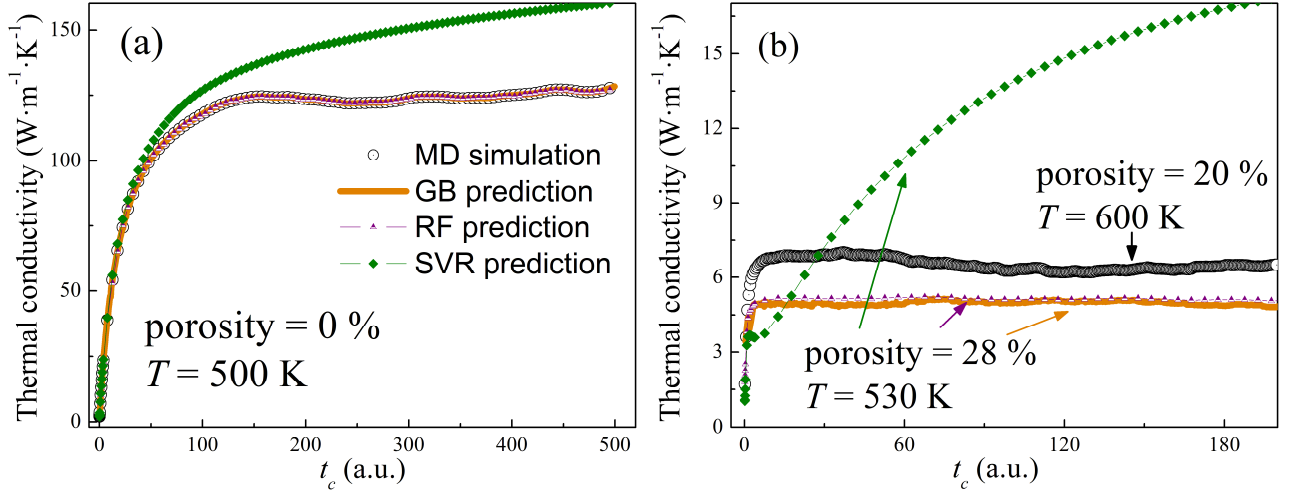

Figure 8. Dependencies of k on t_c, calculated by MD simulations (black circles) and predicted by various ML algorithms for porosity and temperature values that either match the MD simulation case (a) or are close to it (b).

One can see that the outputs of the Random Forest and Gradient Boosting models are comparable, yielding MAPE values of 24% and 22%, respectively, and a median absolute percentage error (APE) of 19% for both. The largest deviations are observed at elevated temperatures and porosity levels. In contrast, the Support Vector Regression model exhibits significantly higher errors, with a median relative error of 50%, exceedingly even the mean value of 48%. These results indicate that SVR is the least suitable approach for estimating thermal conductivity via reconstruction of k (t_c) dependencies.

Let us emphasize once again that the predictions obtained using Symbolic Regression, Random Forest, and Gradient Boosting exhibit characteristic features consistent with general physical considerations: (a) a decrease in thermal conductivity with increasing temperature, (b) modification of the k (T) dependence with increasing disorder, and (c) weakening of the material's ability to transfer thermal energy due to higher porosity. Deviations from these trends are observed only for SVR, further indicating the inappropriateness of this approach.
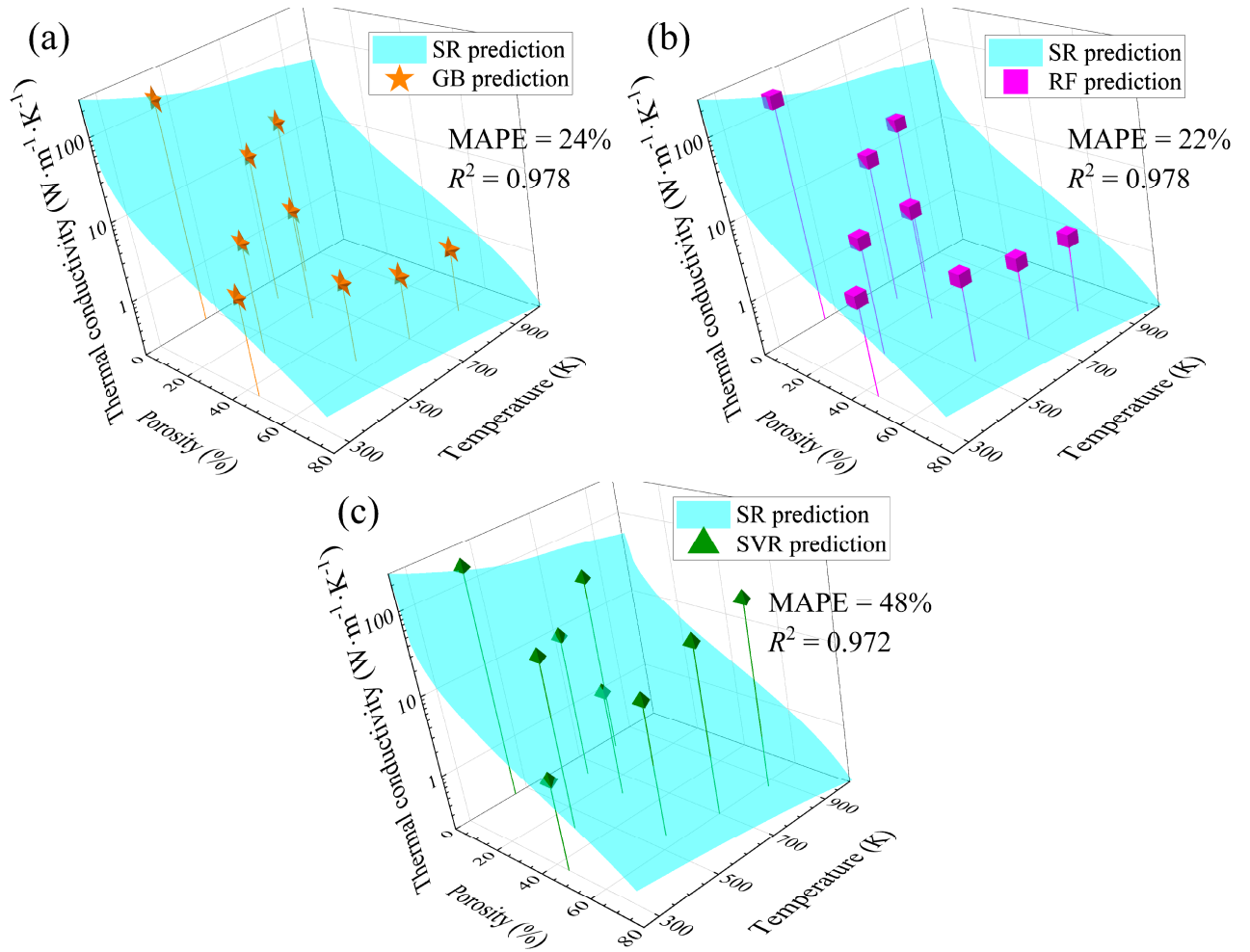
Figure 9. Thermal conductivity values determined from the k (t_c) curves predicted by Gradient Boosting (a), Random Forest (b), and Support Vector Regression (c), compared with the values calculated using Eq. (7). The evaluation metrics were computed under the assumption that Eq. (7) provides the true values.

Conclusion

This study evaluated the suitability of several interatomic potentials for calculating the thermal conductivity of porous silicon via molecular dynamics (MD) simulations and confirmed the adequacy of the Tersoff potential. Thermal conductivity was then computed over a broad range of temperatures and porosity values. Based on these data, a Symbolic Regression algorithm was employed to derive an analytical expression describing the dependence of thermal conductivity on temperature (100–300 K) and porosity (0–80%). Furthermore, it was demonstrated that Random Forest and Gradient Boosting algorithms can reliably estimate thermal conductivity by reconstructing the time dependence of the heat current autocorrelation function. In contrast, Support Vector Regression yielded significantly less accurate results and was deemed unsuitable for this task.

Acknowledgments

References

[1]. Chatterjee S, Paras, Hu H, Chakraborty M. A Review of Nano and Microscale Heat Transfer: An Experimental and Molecular Dynamics Perspective. *Processes*. 2023; 11(9):2769. https://doi.org/10.3390/pr11092769

[2]. Anto Zacharias, Rajesh Baby, Hanna J. Maria, Sabu Thomas. Preparation, characterization, and selection of nano-assisted phase change materials for thermal management and storage applications. *Renewable and Sustainable Energy Reviews*. 2025; 210:115195. https://doi.org/10.1016/j.rser.2024.115195

[3]. V. Lacatena, M. Haras, J.-F. Robillard, S. Monfray, T. Skotnicki, E. Dubois. Phononic engineering of silicon using "dots on the fly" e-beam lithography and plasma etching. *Microelectronic Engineering*. 2014; 121: 131-134. https://doi.org/10.1016/j.mee.2014.04.034

[4]. Siqi Xie, Hongxin Zhu, Xing Zhang and Haidong Wang. A brief review on the recent development of phonon engineering and manipulation at nanoscales. *Int. J. Extrem. Manuf.* 2024; 6(1); 012007. https://doi.org/10.1088/2631-7990/acfd68

[5]. Kuryliuk, V., Tyvonovych, O., & Semchuk, S. Impact of Ge clustering on the thermal conductivity of SiGe nanowires: atomistic simulation study. *Physical Chemistry Chemical Physics*. 2023; 25(8): 6263–6269. https://doi.org/10.1039/d2cp05185k

[6]. Mykola Isaiev, Yuliia Mankovska, Vasyl Kuryliuk, David Lacroix. Thermal transport properties of nanoporous silicon with significant specific surface area. *Appl. Phys. Lett.* 2023; 122 (17): 172201. https://doi.org/10.1063/5.0148434

[7]. D. Lacroix, M. I. Nkenfack, G. Pernot, M. Isaiev. Thermal properties of nanoporous materials, large scale modelling with the use of Monte Carlo phonon transport autocorrelation. *J. Appl. Phys.* 2023; 134 (2): 025101. https://doi.org/10.1063/5.0155582

[8]. Stephen E. Lewis, John R. DeBoer, James L. Gole, Peter J. Hesketh. Sensitive, selective, and analytical improvements to a porous silicon gas sensor. *Sensors and Actuators B: Chemical.* 2005; 110(1): 54-65. https://doi.org/10.1016/j.snb.2005.01.014

[9]. Donghyeok Ma, Da Hoon Kim, Mi Yu, Ye Eun Cho, Hansu Kim. Porous silicon layer overlaid graphite anode materials for fast-charging of lithium-ion batteries. *Journal of Power Sources*. 2025; 645:237199. https://doi.org/10.1016/j.jpowsour.2025.237199

[10]. Dzhafarov, T., Bayramov, A. Porous Silicon and Solar Cells. In: Canham, L. (eds) Handbook of Porous Silicon. Springer, Cham. 2017. https://doi.org/10.1007/978-3-319-04508-5_95-2

[11]. Gerhard Müller, Alois Friedberger, Kathrin Knese. Handbook of Silicon Based MEMS Materials and Technologies. William Andrew Publishing. 2010. https://doi.org/10.1016/B978-0-8155-1594-4.00025-5

[12]. U. Bernini, S. Lettieri, P Maddalena, R. Vitiello and G. Di Francia. Evaluation of the thermal conductivity of porous silicon layers by an optical pump-probe method. *J. Phys.: Condens. Matter.* 2001; 13: 1141. https://doi.org/10.1088/0953-8984/13/5/327

[13]. Pritam Sharma, John Dell, Giacinta Parish, Adrian Keating. Engineering $1/f$ noise in porous silicon thin films for thermal sensing applications. *Microporous and Mesoporous Materials.* 2021; 324: 111302. https://doi.org/10.1016/j.micromeso.2021.111302

[14]. Nguyen Van Toan, Yijie Li, Truong Thi Kim Tuoi, Nuur Syahidah Sabran, Jun Hieng Kiat, Ioana Voiculescu, Takahito Ono. Thermoelectric generator using nanoporous silicon formed by metal-assisted chemical etching method. 2025. *Energy Conversion and Management.* 2025; 323:119268. https://doi.org/10.1016/j.enconman.2024.119268

[15]. Jin Fang, Laurent Pilon; Scaling laws for thermal conductivity of crystalline nanoporous silicon based on molecular dynamics simulations. *J. Appl. Phys.* 2011; 110(6): 064305. https://doi.org/10.1063/1.3638054

[16]. Y. He and G. Galli. Microscopic origin of the reduced thermal conductivity of nanoporous Si. *Phys. Rev. Lett.* 2012; 108: 215901. https://doi.org/10.1103/PhysRevLett.108.215901

[17]. Jin Fang, Laurent Pilon; Tuning thermal conductivity of nanoporous crystalline silicon by surface passivation: A molecular dynamics study. *Appl. Phys. Lett.* 2012; 101 (1): 011909. https://doi.org/10.1063/1.4733352

[18]. Mykola Isaiev, Nataliia Kyrychenko, Vasyl Kuryliuk, David Lacroix; Features of phonon scattering by a spherical pore: Molecular dynamics insight. *Appl. Phys. Lett.* 2024; 124 (14): 142202. https://doi.org/10.1063/5.0200817

[19]. Ryan Jacobs, Dane Morgan, Siamak Attarian *et al*. A practical guide to machine learning interatomic potentials – Statusand future. *Current Opinion in Solid State & Materials Science.* 2025, 35: 101214. https://doi.org/10.1016/j.cossms.2025.101214

[20]. Guanjie Wang, Changrui Wang, Xuanguang Zhang, Zefeng Li, Jian Zhou, Zhimei Sun. Machine learning interatomic potential: Bridge the gap between small-scale models and realistic device-scale simulations. *iScience.* 2024, 27:109673. https://doi.org/10.1016/j.isci.2024.109673

[21] Hoang-Giang Nguyen, Thanh-Dung Le, Hong-Giang Nguyen, Te-Hua Fang. Mechanical properties of AlCoCrCuFeNi high-entropy alloys using molecular dynamics and machine learning. *Materials Science & Engineering R.* 2024, 160: 100833. https://doi.org/10.1016/j.mser.2024.100833

[22] Omarelfarouq Elgack, Belal Almomani, Junaidi Syarif, Mohamed Elazab, Mohammad Irshaid, Mohammad Al-Shabi. Molecular dynamics simulation and machine learning-based analysis for predicting tensile properties of high-entropy FeNiCrCoCu alloys. *Journal of Materials Research & Technology.* 2023, 25: 5575. https://doi.org/10.1016/j.jmrt.2023.07.023

[23]. Luo Y., Li M., Yuan H. et al. Predicting lattice thermal conductivity via machine learning: a mini review. *npj Comput Mater.* 2023; 9:4. https://doi.org/10.1038/s41524-023-00964-2

[24] Liben Guo, Yuanbin Liu, Lei Yang, and Bingyang Cao. Lattice dynamics modeling of thermal transport in solids using machine-learned atomic cluster expansion potentials: A tutorial. *J. Appl. Phys*. 2025, 137 (8): 081101. https://doi.org/10.1063/5.0251119

[25] Xianqing Liu, Fei Liang, Shule Liu, Gechuanqi Pan, Jing Ding, Jianfeng Lu. NaCl-KCl-CaCl2 molten salts for high temperature heat storage: Experimental and deep learning molecular dynamics simulation study. *Solar Energy Materials & Solar Cells*. 2025, 280: 113275. https://doi.org/10.1016/j.solmat.2024.113275

[26] Yao Du, Penghua Ying, Jin Zhang. Prediction and optimization of the thermal transport in hybrid carbon-boron nitride honeycombs using machine learning. *Carbon*. 2021, 184: 492. https://doi.org/10.1016/j.carbon.2021.08.035

[27] Prabudhya Roy Chowdhury and Xiulin Ruan. Unexpected thermal conductivity enhancement in aperiodic superlattices discovered using active machine learning. *npj Comput Mater.* 2022; 8:12. https://doi.org/10.1038/s41524-022-00701-1

[28] Jing Wan, Jin-Wu Jiang, Harold S. Park. Machine learning-based design of porous graphene with low thermal conductivity. *Carbon*. 2020, 157: 262. https://doi.org/10.1016/j.carbon.2019.10.037

[29]. A. P. Thompson, H. M. Aktulga, R. Berger, D. S. Bolintineanu, W. M. Brown, P. S. Crozier, P. J. in 't Veld, A. Kohlmeyer, S. G. Moore, T. D. Nguyen, R. Shan, M. J. Stevens, J. Tranchida, C. Trott, S. J. Plimpton. LAMMPS - a flexible simulation tool for particle-based materials modeling at the atomic, meso, and continuum scales. *Comp Phys Comm*. 2022; 271:10817. https://doi.org/10.1016/j.cpc.2021.108171

[30] S. Moser, C. Kenel, L.A. Wehner, R. Spolenak, D.C. Dunand. 3D ink-printed, sintered porous silicon scaffolds for battery applications. *Journal of Power Sources*. 2021; 507: 230298. https://doi.org/10.1016/j.jpowsour.2021.230298

[31] Zaichun Liu, Xinhai Yuan, Shuaishuai Zhang, Jing Wang, Qinghong Huang, Nengfei Yu, Yusong Zhu, Lijun Fu, Faxing Wang, Yuhui Chen & Yuping Wu. Three-dimensional ordered porous electrode materials for electrochemical energy storage. *NPG Asia Materials*. 2019; 11: 12. https://doi.org/10.1038/s41427-019-0112-3

[32] Dimitrios Angelis, Filippos Sofos, Theodoros E. Karakasidis. Artificial intelligence in physical sciences: symbolic regression trends and perspectives. *Archives of Computational Methods in Engineering*. 2023, 30:3845. https://doi.org/10.1007/s11831-023-09922-z

[33] F. Sofos, C. Dritselis, S. Misdanitis, T. Karakasidis, D. Valougeorgis. Computation of flow rates in rarefied gas flow through circular tubes via machine learning techniques. *Microfluidics and Nanofluidics*. 2023 27:85. https://doi.org/10.1007/s10404-023-02689-6

[34] Miles Cranmer. Interpretable Machine Learning for Science with PySR and SymbolicRegression.jl. arXiv:2305.01582. https://doi.org/10.48550/arXiv.2305.01582

[35]. B.-J. Lee. A modified embedded atom method interatomic potential for silicon. *Calphad.* 2007; 31(1): 95-104. https://doi.org/10.1016/j.calphad.2006.10.002

[36]. J. Tersoff. Modeling solid-state chemistry: Interatomic potentials for multicomponent systems. *Physical Review B.* 1989; 39(8): 5566-5568. https://doi.org/10.1103/physrevb.39.5566

[37]. J.F. Justo, M.Z. Bazant, E. Kaxiras, V.V. Bulatov, and S. Yip. Interatomic potential for silicon defects and disordered phases. *Physical Review B.* 1998; 58(5): 2539-2550. https://doi.org/10.1103/physrevb.58.2539

[38]. F.H. Stillinger, and T.A. Weber. Computer simulation of local order in condensed phases of silicon. *Physical Review B.* 1985; 31(8): 5262-5271. https://doi.org/10.1103/physrevb.31.5262

[39]. Yongjin Lee and Gyeong S. Hwang. Force-matching-based parameterization of the Stillinger-Weber potential for thermal conduction in silicon. *Physical Review B.* 2012; 85: 125204. https://doi.org/10.1103/PhysRevB.85.125204

[40]. A.P. Thompson, L.P. Swiler, C.R. Trott, S.M. Foiles, G.J. Tucker. Spectral neighbor analysis method for automated generation of quantum-accurate interatomic potentials. *Journal of Computational Physics.* 2015; 285: 316-330. https://doi.org/10.1016/j.jcp.2014.12.018

[41]. A.V. Inyushkin, A.N. Taldenkov, J. W. Ager, E. E. Haller, H. Riemann, N. V. Abrosimov, H.-J. Pohl, P. Becker. Ultrahigh thermal conductivity of isotopically enriched silicon. *J. Appl. Phys.* 2018; 123 (9): 095112. https://doi.org/10.1063/1.5017778